Pulse Compression for Long Spread Spectrum Signals Application in Air-Coupled Ultrasonic Thickness Resonance Spectroscopy

Linas Svilainis, *Senior Member, IEEE*, and Muhammad Tayyib

***Abstract*—Interfering reflections occur due to air impedance mismatch from sample and transducer in noncontact resonance ultrasound spectroscopy (NC-RUS) measurements. The transducer is in close vicinity to the sample in order to ensure low attenuation in the air and flat wavefront. Therefore, interfering reflections are at 30–100 μs distance from the useful signal. Pulse excitation is used to avoid the overlap that can distort the measurement. A short pulse is required to ensure a broadband excitation, but such a pulse is low energy. Air-to-sample impedance mismatch further reduces signal energy and SNR. Therefore, very high-voltage excitation and averaging is required. High-voltage excitation increases nonlinearity effect in air, averaging increases measurement time. Long spread spectrum (SS) signals can achieve high SNR, avoid distortion in air, and expand the bandwidth available for analysis. However, long SS signals will overlap. Here, it was demonstrated that the pulse compression (PuC) using matched filter (MF) is not suitable: the correlation sidelobes overlap with interfering reflections and bias errors of NC-RUS measurements increase. Solution proposed for PuC uses inverse filter (IF). Such compressed signal corresponds to ideal pulse excitation (uniform spectrum) and has no sidelobes. If the spectral content of the SS needs to be preserved, then the PuC result can be gated and decompressed back. It was demonstrated that errors can be significantly reduced in such a case. For example, 0.008% sample density estimation bias error is achieved in case of 350 μs long excitation compared to 2.42% when using MF or 2.1% in case of mismatched filter (MMF), a 300 times reduction.**

***Index Terms*—Inverse filter (IF), matched filter (MF), noncontact resonance ultrasound spectroscopy (NC-RUS), pulse compression (PuC), spread spectrum (SS) signals.**

I. Introduction

THE direct relationship between wave propagation and the material mechanical properties is the reason why ultrasonic measurements are so popular. In general, ultrasonic measurement fundamentally involves the transduction of the electrical energy into acoustical waves, coupling those waves into the test sample, and then conversion back to receiving electronics. Analysis of reflected or transmitted signals allows to characterize the material [1], [2]. Air-coupled ultrasound (ACU) uses air as a coupling medium to inject the signal into the sample [3], [4], [5], [6]. It is noncontact, there is no need for water-tight, corrosion-resistant probes, cables, scanning equipment. Can be carried out on samples that are fragile, soft, or cannot be wetted. The value of ACU was already verified for studies of art pieces [3], nondestructive testing [4], [5], [6], material properties measurement [7], imaging [8], production line control [9], gas flow measurement [10], food products [11], or plant studies [12].

However, the acoustic impedance of air is about 410 Rayl, significantly lower than that of most solids and piezomaterials used for transduction (1–30 MRayl) [13], [14], [15], [16]. As ultrasound waves travel from piezoelement to air, then air to sample and then back, most energy will be reflected at the interfaces. Thus, the transmitted signal is significantly reduced [17]. For example, the transmission loss for the aluminum plate is 87 dB. Also, attenuation in air is high and frequency-dependent [18], [19]. At 100 kHz, the attenuation over 100 mm of air is relatively modest, about 0.3 dB, meanwhile at 5 MHz it is 400 dB, but 40 dB at 10 mm distance. Difference of speed of sound in air (343 m/s) and sample (1500–12 000 m/s for solids) defines that range of incident angles is small, for example, for aluminum critical angle (total reflection) is mere 3°. If a spherical wave hits the sample surface, only small fraction of wavefront will penetrate to sample. This leads to requirement to operate at flat wavefront (i.e., near field).

Therefore, air-coupled measurements are typically carried out at short distances, at low frequencies (10's of kHz to a few megahertz) and operation is at tens of millimeters, where signal losses are more manageable [20].

Significant progress has been made in improving the sensitivity of ultrasonic transducers by better match to air [21], [22], [23], [24], yet even novel transducers still lack transduction sensitivity and bandwidth.

The axial resolution is defined by the signal bandwidth, which, in turn, is limited by the transducer bandwidth. If the thickness of a thin sample needs to be measured, it is usually required that the axial resolution be better than the sample thickness. If reverberations within the sample thickness overlap, such a measurement becomes impossible, even with pulse compression applied.

Noncontact resonance ultrasound spectroscopy (NC-RUS) was proposed as a remedy when reverberations within the

Received 5 January 2026; revised 10 February 2026; accepted 9 March 2026. Date of publication 20 March 2026; date of current version 1 April 2026. This work was supported by the Research Council of Lithuania (LMTLT) under Grant S-MIP-23-133. The Associate Editor coordinating the review process was Dr. Alvaro Hernandez. *(Corresponding author: Linas Svilainis.)*

The authors are with the Electronics Engineering Department, Kaunas University of Technology, 51368 Kaunas, Lithuania (e-mail: linas.svilainis@ktu.lt; muhammad.tayyib@ktu.edu).

Digital Object Identifier 10.1109/TIM.2026.3676189

sample thickness overlap [33], [34]. Overlapping produces constructive and destructive interferences, which are addressed as thickness resonances. The ultrasound propagation time can be deduced from the peak frequency, and the thickness can be estimated if the velocity is known [33]. NC-RUS performs in a more advanced manner [34]. Two through-transmission measurements are carried out: 1) calibration measurement, when the path between transducers is free from obstacles and 2) sample measurement, when a sample is inserted between transducers. The thickness resonance of the plate produces resonant peaks in the transmission spectrum, which is related to the thickness of the sample and the ultrasound velocity of the sample. Additionally, there is a signal shift in time between calibration and sample measurements, which are also related to thickness and velocity. These two independent values allow for the simultaneous estimation of the sample thickness and velocity. The width of peaks and the depth of valleys is related to acoustic impedance and attenuation. Then, the thickness, density, ultrasound velocity, and attenuation of the sample can be estimated simultaneously by inverse solution using the transmission model of the sample [17].

NC-RUS is extremely demanding for SNR and bandwidth. High SNR is required because signal transmission losses are high and the quality of the attenuation and density estimation (inverse solution) largely depends on how large the SNR is in the resonance valley, where the attenuation is the highest. On the other hand, position of the resonant peaks depends on the speed of sound and the thickness of the sample. The estimation quality for the thickness and speed of sound in the sample degrades if the peaks are not covered by the transducer passband. Finally, the estimation of the frequency dependence of the attenuation in the sample is largely affected by the available bandwidth. Therefore, usually NC-RUS is carried out using several pairs of ultrasonic transducers with different center frequency in order to get a wideband measurements and single, short pulse excitation [12], [34], [35], [36].

Short pulse excitation is preferred [1], [3], [4], [8], [11], [12], [25] for two reasons: 1) to get a broadband excitation and 2) to avoid the overlapping with interfering reflections between the sample and transducer. However, short signal does not have enough energy, which is extremely important for ACU due to attenuation and transmission losses. SNR can be improved by increasing the pulse amplitude, but there are physical limits for maximum excitation voltage. High excitation voltage is also increasing the nonlinearity in air [45] and spectrum becomes distorted. Therefore, averaging is used to increase SNR, leading to longer measurement time.

Spread spectrum (SS) signals have been proposed as a solution [26], [27], [28], [29]: signals can be very long, that is, large SNR can be achieved and bandwidth can be arbitrary broad and uniform. SS signals are more energy-efficient and can deliver wide bandwidth, avoiding high voltage use for excitation to reduce the nonlinearity in air. Furthermore, SS signal spectral shape can be altered by using amplitude modulation (AM) of linear frequency modulation (LFM) chirp [37] to compensate the lack of transduction bandwidth. Better solutions, using nonlinear frequency modulation (NLFM) [38], [39] or arbitrary pulsewidth and position (APWP) [40] signals, were proposed for excitation. It was demonstrated [41], [42], [46] that bandwidth of the received signal can be broadened by pushing the energy of the excitation signal into frequencies where transduction losses are high.

However, SS application in NC-RUS is limited by interfering reflections between the sample and transducer. Reverberation time is short, usually 30–100 μs, because of small operation distance. Reflections are large, with amplitude comparable to useful signal, due to significant air-sample and air-transducer acoustic impedance mismatch. All SS implementations on NC-RUS explored so far were using signal duration which was shorter or comparable to sample-transducer reverberation time. Such approach limits the SS duration to approximately 50 μs. Long SS signal duration is essential to accumulate sufficient energy. Also, spectrum programming flexibility of APWP signal depends on signal length: the longer is the signal, the more flexible and more accurate is the spectral shaping. Solution seems trivial: pulse compression (PuC). SS signals can be compressed using matched filter (MF) [29], [30]. However, pulse compression produces sidelobes. For general imaging or ranging, this issue is not significant, to some extent it can be mitigated by SS signal envelope tapering in time [32] or mismatched filter (MMF) application [31]. Values of such approach have been demonstrated in ranging [26], sonar [27], multiphase flow [28], biomedical [31] imaging, or material inspection [29].

Yet, NC-RUS is based on the accuracy of the signal temporal and spectral content. Reverberation within sample produces ringdown in sample signal tail. Decay rate of this ringdown contains the information on sample acoustic impedance and attenuation. Sidelobes of the interfering transducer-sample reflections will overlap with tail ringdown, resulting in bias errors of impedance and attenuation estimation. Overlapping sidelobes will also alter sample signal shift in time and its amplitude, resulting in thickness and sample velocity estimation errors.

The objective of this article was to develop a PuC technique, suitable for long SS signals application in NC-RUS and compare its performance with other candidates.

Novelty of the approach, proposed here is in application of inverse filter (IF) for pulse compression. IF and Wiener filter (WF) usually are used for bandwidth deficiency compensation in order to improve the range resolution [46], [50]. That is, major concern is the compensation of transduction spectral shape by altering the excitation signal. But required spectral shape of the excitation signal cannot be achieved even by using AM modulation of SS signal, spectral ripples remain, and sidelobes are introduced [46], [50].

In this article IF application is different: aim is to remove the sidelobes by maintaining the transduction response in the received signal, by using the excitation signal as reference. There are two types of MF sidelobes: near-range and far-range. Near-range sidelobes are caused by rectangular shape of chirp spectrum. The reason of the far-range sidelobes are Fresnel ripples of LFM [31]. Situation is worsened if, as in this work, rectangular pulse sequences are used. Rectangular sequences are more energy-efficient and require less complicated electronics, but spectral ripples are higher and more

complex, resulting in further increase of correlation sidelobes. MF amplifies these effects, while IF deconvolves the excitation from received signal.

It was already noted that application of IF for PuC can eliminate or minimize the sidelobes [49], [51], [52]. Sidelobes are minimized when excitation signal is used as reference, because in such cases both phase and magnitude ripples, inherent to LFM, are removed. However, research [49], [51], [52] used phase shift keying (PSK) coded sequences, ignoring LFM. We think that PSK signals are not the best candidate for IF. The reason is in its spectrum and inherent IF property to increase the noise at frequencies where reference signal spectral components are low. Spectrum of PSK sequences approximately follows the spectrum of the chip, that is, is similar to *sinc* function. If *sinc* center is matched to transducer center frequency, noise is increased at frequencies where SNR is already low (at roll-off and stopband frequencies). Therefore, application of IF for PuC is considered as reducing SNR compared to MF. But, if LFM or transduction-losses-compensated NLFM or APWP signals [41], [42], [46] are used for excitation, SNR is improved at passband edges. If bandwidth for coverage is chosen to cover −20 dB bandwidth, sufficient SNR can be ensured at passband roll-off. Furthermore, NC-RUS measurement is using separate transmit and receive transducers. In such cases, excitation signal can be much longer, that is, larger time-bandwidth (TB) product can be achieved. Still, noise gain will be produced at the frequencies that are not covered by LFM or APWP excitation. Then additional bandpass filter can be added to IF [49]. This additional filter will not distort the compressed signal if its passband is set at −20 dB transducer bandwidth and, as was proposed above, −20 dB transducer bandwidth is covered by excitation. Result can be considered as an intermediate between inverse and WF. Essential that PuC using IF corresponds to excitation using ideal pulse excitation (uniform spectrum). That is, signal received is similar to very broadband pulse excitation with SNR significantly improved.

Another problem to solve is related to gating of the signals with long sample reverberation time. NC-RUS is usually using spectral domain fitting of transmission spectrum [12], [33], [34], [35], [36]. Then, both sample and calibration signals need to be gated in order to get rid of interfering transducer-sample reflections. Even IF-compressed sample signal contains sample reverberation. If decay of this reverberation is long, gating of interfering reflection will cancel the tail too early and spectral content will be distorted. If such signal if used for fitting, estimation results will be biased. One more novelty used here is that fitting is performed on sample signal in time domain. In such cases, gating is not required: fitting is performed over section of signal that does not contain interfering reflections. Such approach allows to reduce bias errors with PuC using IF, this is demonstrated in Section III.

Removal of the spectral content of the excitation signal is not always desired. If spectral content of the excitation signal was altered by pushing the energy into frequencies, where transduction losses are high this results in broadened bandwidth of the received signal [41], [42], [46]. But application of IF results in this effect removal. Important to point out that SNR is still improved by the amount of transduction losses compensation placed in excitation spectrum shape, because IF also alters the noise spectrum, this is demonstrated is Section II-C. Yet, frequency components with larger spectral losses contribute less to sample parameters estimation because fitting is on sample signal.

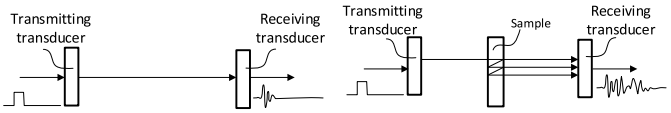

Fig. 1. NC-RUS setup for calibration (left) and sample (right) measurement.

Another novelty proposed here is that IF can be used only to produce the PuC; after compressed signal is obtained, interfering reflections are gated out and signal is decompressed back and used for fitting.

Contributions of this work are as follows.

1) *Sidelobe-Free IF-Based PuC:* Achieves high-SNR, ideal-pulse-equivalent response without the sidelobes typical of MF, MMF, and WF, reducing NC-RUS bias errors.
2) *Time-Domain NC-RUS Fitting:* Decouples sample reverberations from interfering transducer–sample reflections, enabling characterization despite overlapping.
3) *Spectral Integrity:* Compression-gating-decompression strategy can preserve spectral shape imposed by excitation.
4) *Performance Evaluation:* Bias errors were analyzed for both proposed and conventional PuC techniques under various spectral programming and energy combinations.

Section II is used for problem analysis and introduction of the processing algorithms. Section III is used for all PuC candidates' performance evaluation in NC-RUS measurements using both simulation and real experiment. Section IV is used for discussion and details analysis.

II. Problem Analysis

Problem analysis is based on experimental measurements. A 2 mm thick polycarbonate plate was measured. Two air-coupled 20 mm diameter, 650 kHz center frequency transducers [43] (designed and manufactured by CSIC, Spain) in through-transmission setup (Fig. 1) were used to collect the data required for NC-RUS: calibration (no sample in between) and sample (sample inserted between transducers) signals.

Transducers were spaced 34 mm apart and excitation used a single 100 ns duration rectangular pulse. Calibration measurement is taken using 10 V excitation and sample measurement used 20 V excitation. Low excitation voltage was used to avoid nonlinearities in air: as reported in [45], nonlinearities appear at voltages above 35 V.

Transduction response can be evaluated by studying the calibration measurement response presented in Fig. 2. Note the vertical axis (mV/V): signal at receiving transducer output was normalized to excitation voltage on transmitting transducer in order to reflect the transduction sensitivity.

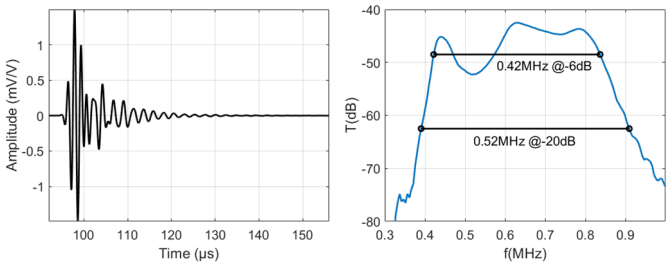

Fig. 2. Calibration signal in time (left) and transmission AC response (right) in case of 100 ns pulse excitation. Horizontal lines indicate the bandwidth at −6 and −20 dB.

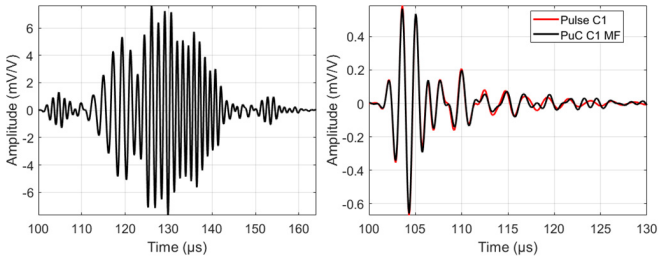

Fig. 3. Calibration signal in case of 50 μs long LFM excitation (left) and after pulse compression using MF (right). Red-comparison to pulse (scaled).

Transduction bandwidth is 420 kHz (65%) at −6 dB and 520 kHz (81%) at −20 dB level. Insertion loss varies from −52 to −42 dB within a passband.

Calibration signal in time [Fig. 2 (left)] is quite short as for air-coupled transducer: approximately 3 μs at 50% and 30 μs ringdown. With 34 mm distance between transducers, reverberation time is approximately 200 μs, so no interference with transducer-transducer reflections occurs. However, as it was mentioned before, short signal does not have sufficient energy to ensure high SNR after sample penetration, which is extremely important in NC-RUS measurements.

SNR can be improved by LFM chirp excitation.

A. PuC Using Standard Approach

Calibration signal, obtained using LFM excitation is presented in Fig. 3.

Fig. 3 (left) is the calibration signal, obtained using 250 kHz–1.1 MHz range, 50 μs long 10 V LFM chirp (rectangular, bipolar signal), and Fig. 3 (right) is the result of pulse compression (excitation signal as reference) using MF

$$C_{\mathrm{MF}}(\omega) = C(\omega)\,conj(G(\omega))$$
$$S_{\mathrm{MF}}(\omega) = S(\omega)\,conj(G(\omega)) \quad (1)$$

where $C(\omega)$ and $S(\omega)$ are calibration and sample signals, $G(\omega)$ is excitation signal, $C_{\mathrm{MF}}(\omega)$ and $S_{\mathrm{MF}}(\omega)$ are calibration and sample signals after MF in frequency domain.

Signal amplitude increased after PuC, but Fig. 3 (right) signal was shifted and scaled for comparison to pulse excitation (red: pulse excitation and black: LFM excitation after PuC using MF). At first glance, PuC using MF produces desired result: SNR was increased, signal was compressed to same shape as with single pulse excitation. Yet, additional

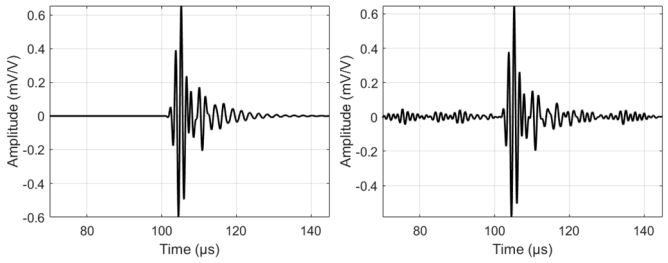

Fig. 4. Comparison of pulse excitation (left) and MF compressed LFM (right). Compressed signal normalized.

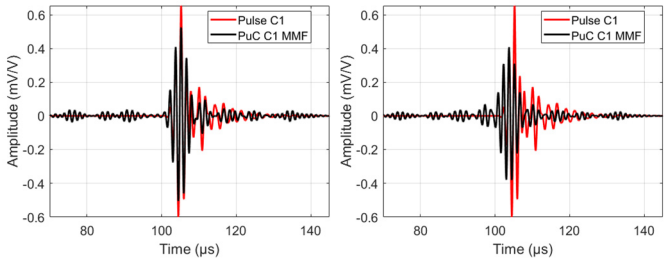

Fig. 5. Mismatched (Blackman–Harris) filter-based PuC when reference signal is: excitation code (left) or calibration signal (right).

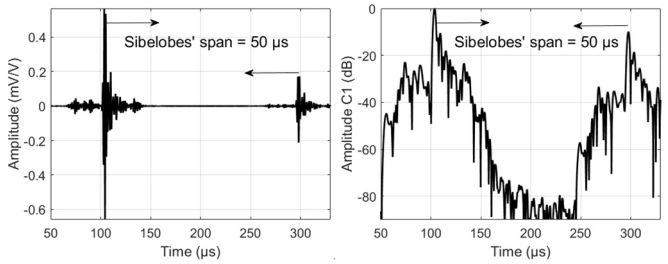

Fig. 6. MF compressed calibration signal (left) and its envelope (right).

ripples appear in compressed signal. Results for pulse and LFM excitation are plotted separately in Fig. 4 at larger time scale.

Now, it can be noted that compression result differs from pulse excitation. Actually, situation is essentially worse [see Fig. 4 (right)]: correlation sidelobes [31], [32] appear on both sides of the compressed pulse (mainlobe).

Application of MMF [31], using minimum four-term Blackman–Harris window $BH(\omega)$

$$C_{\mathrm{MMF}}(\omega) = BH(\omega)\,C(\omega)\,conj(G(\omega))$$
$$S_{\mathrm{MMF}}(\omega) = BH(\omega)\,S(\omega)\,conj(G(\omega)) \quad (2)$$

does not solve the problem [see Fig. 5 (left)], only makes situation worse: note how much distorted in the mainlobe, compared to pulse excitation.

Choice of reference signal does not change the situation: Fig. 5 (left) is the PuC result when excitation signal is used as reference; Fig. 5 (right) is the result of calibration signal use for PuC (~ autocorrelation). Result can be expected: MMF is aimed at near-range sidelobes reduction at expense of central lobe broadening. Actual problem can be seen in Fig. 6,

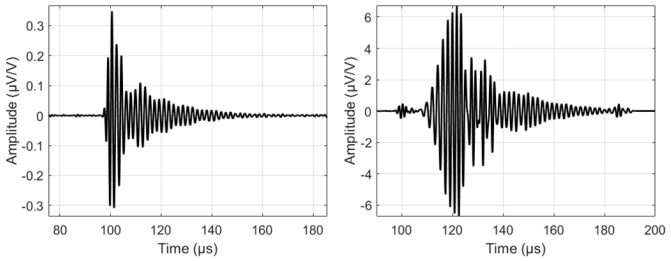

Fig. 7. Sample signal in time in case of 100 ns pulse (left) and 50 µs long LFM (right) excitation.

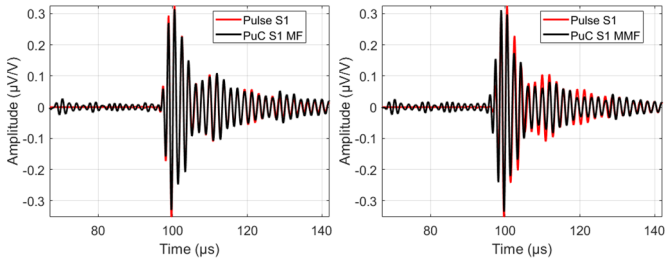

Fig. 9. Comparison of sample signal PuC result using MF (left) and MMF (right) for 50 µs long LFM. Normalized to pulse.

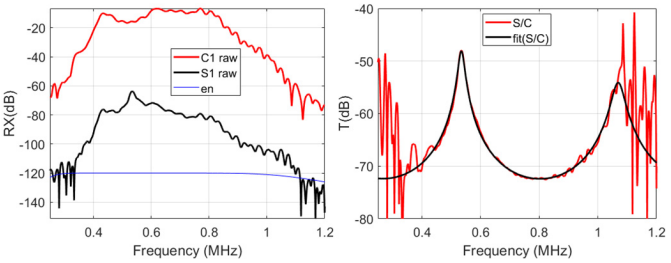

Fig. 8. Spectra of gated calibration (red), sample (black) and noise (blue) signals (left). Sample transmission response measured (red) and fit (black) (right).

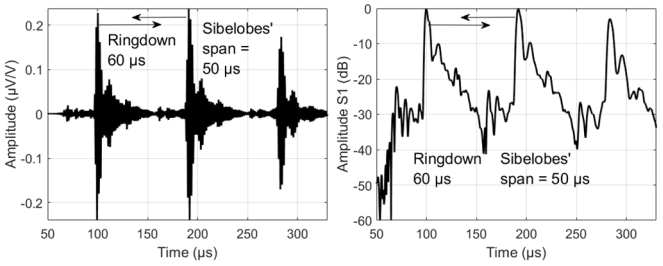

Fig. 10. MF compressed sample signal (left) and its envelope (right) for 50 µs long LFM.

where even broader time range is used. Interfering transducer-transducer reflections appear at 300 µs (reverberation time is 200 µs), but sidelobes span by LFM chirp duration, 50 µs, from both first burst and interfering reflection. This means that only 100 µs long LFM chirp can be used for excitation in order to maintain reliable gating. Use of longer excitation signals will result in overlapping if MF PuC is used.

Situation is even worse for the sample signal (Fig. 7): 1) there is a reverberation in the sample which increases the ringdown time to approximately 60 µs and 2) sample-transducer reverberation time is more than twice shorter, 93 µs (versus 200 µs for calibration signal).

It can be noted, that sample signal is much smaller (µV/V versus mV/V for calibration) due to significant sample impedance mismatch to air. Note that signal is plotted over wider time interval than calibration signal (Fig. 2) in order to reflect the signal ringdown, caused by reverberation in sample. This sample reverberation carries essential information about the sample impedance and attenuation. If sample and calibration signals are gated to remove the interfering reflections transferred to frequency domain, a sample transmission response is obtained (see Fig. 8). Fig. 8 (left) represents the calibration, sample, and noise spectra. Noise spectral density (label "en," blue curve in plots) was measured for sample setup, using technique described in [44] and can be used for visual SNR estimation. Fig. 8 (right) represents sample transmission response obtained from experimental measurements (red) and estimated using NC-RUS (black) inverse solution using [17].

Fig. 8 results were obtained using same 50 µs long 250 kHz–1.1 MHz LFM excitation. Signals were not compressed, because sample-transducer reverberation time (93 µs) is less than excitation burst length (50 µs) and ringdown time (60 µs). The gate can be positioned just before start of interfering reflection (at 90 µs distance). Yet, if MF PuC is used, the sidelobes appear (Fig. 9) which objects the proper gating.

Problem can better be seen at larger time scale, see Fig. 10.

When sample is inserted, propagation distance is 16 mm which corresponds to approximately 93 µs reverberation time. This means that if 50 µs long SS signal is used for excitation, sidelobes of interfering reflection will end at 43 µs (93–50 µs). Meanwhile, ringdown due to sample reverberation is 60 µs. Overlapping will occur, making the gating impossible (see Fig. 10). The fitting (inverse solution) is usually done in frequency domain [12], [33], [34], [35], [36]. If gate is set at position where sample reverberation is not decayed sufficiently, a spectrum convolution with *sinc* function will occur. Sample parameters estimation will develop bias errors.

B. Solution for Tail: Time Domain Fitting

Slightly modified fitting procedure is proposed to avoid the need of signal gating and transformation to frequency domain.

Transmission through the sample can be described by [17]

$$T'(\omega) = \frac{-Z_{\text{air}}Z_{\text{s}}}{-2Z_{\text{air}}Z_{\text{s}}\cos(k'h) + j\left(Z_{\text{air}}^2 + Z_{\text{s}}^2\right)\sin(k'h)} \tag{3}$$

where Z_{air} is the acoustic impedance of the air, Z_{s} is the acoustic impedance of the sample, h is the sample thickness, and k' is the complex wavenumber

$$k' = \frac{\omega}{c_{\text{s}}} - j\alpha \tag{4}$$

where $c_{\text{s}}$is the ultrasound velocity in the sample, and α is the acoustic attenuation in sample, defined as

$$\alpha = \alpha_0 \cdot \left(\frac{f}{f_0}\right)^n \tag{5}$$

f_0 is the normalization frequency. The impedances Z_{air} and Z_s

$$Z_{\text{air}} = c_{\text{air}} \cdot \rho_{\text{air}}, \quad Z_s = c_s \cdot \rho_s \tag{6}$$

where c_{air} is the speed of sound in air, and ρ_{air} is the air density.

Usually, as per [12], [33], [34], [35], [36], measured sample transmission response (Fig. 7 red) is used against (3), and sample parameters $x = (h, c_s, n, \rho_s$ and $\alpha)$ are modified until best fit of (3) to measured sample transmission AC response is obtained.

Approach proposed here is different: Sample signal is derived from calibration signal using

$$S_{\text{mod}}(\omega) = C(\omega)\, T(\omega)\, e^{j\omega h/c_{\text{air}}} \tag{7}$$

where $e^{j\omega h/cair}$ is to account the shift due to the air replacement with the sample material over thickness h.

Sample parameters $x = (h, c_s, n, \rho_s$ and $\alpha_0)$ then are estimated by solving the inverse problem of (7). The inverse solution is obtained by minimizing the difference between the simulated s_{mod} and experimentally measured s in time domain

$$x = \arg\min \sum_{i=n_1}^{n_2} \left(\frac{s_{\text{mod}}(x)_i - s_i}{s_i} \right)^2 \tag{8}$$

where n_1 and n_2 are sample numbers of fitting range.

In such case convolution with *sinc* function is avoided and sample parameters estimation can be carried out. Gating is not used, only calculation is carried out within the predefined range $[n_1, n_2]$, where there is no overlapping. Values for n_1 and n_2 are obtained from geometry used (distance between transducers), speed of sound in air and sampling frequency.

However, this solution is efficient only for short excitation signal durations (approximately below 50 μs). Longer excitation signals are preferred in order to obtain higher SNR. Higher SNR would provide lower estimation errors, wider frequency range with SNR > 0 or can be used for spectral losses compensation [40], [41], [42]. If longer (>100 μs) excitation signals are used, sidelobes of interfering reflection will cover the whole signal (refer Fig. 10) and fitting will contain sidelobes, which will result in bias errors. For very long ones (e.g., 300 μs), overlapping sidelobes will also come from second, third, fourth reflection, and so forth (refer Fig. 10). Inverse solution still can be found, but bias errors will increase.

C. Solution for Sidelobes: PuC Using IF

The far-range sidelobes are caused by Fresnel ripples of LFM chirp [31], especially the rectangular version, used here. PuC using MF only amplifies this effect. Remedy proposed here is to use the IF for PuC

$$C_{\text{IF}}(\omega) = W(\omega)\, C(\omega)/G(\omega)$$
$$S_{IF}(\omega) = W(\omega)\, S(\omega)/G(\omega). \tag{9}$$

Same as above, reference signal $G(\omega)$ is excitation code or voltage, measured on transmitting transducer clamps. Filter $W(\omega)$ is optional, intended for noise reduction in low-SNR regions. Essential, that IF deconvolves the excitation from received signal so Fresnel ripples of LFM chirp are removed.

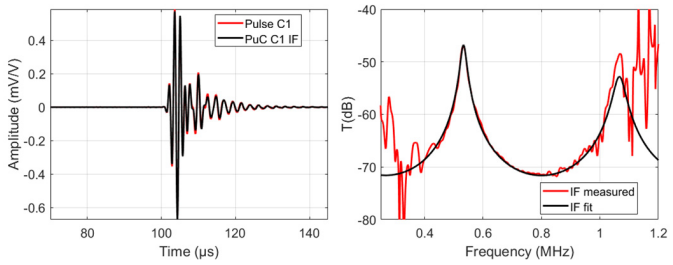

Fig. 11. Calibration signal in case of 350 μs long LFM excitation after PuC using IF (left) and resulting sample transmission (right).

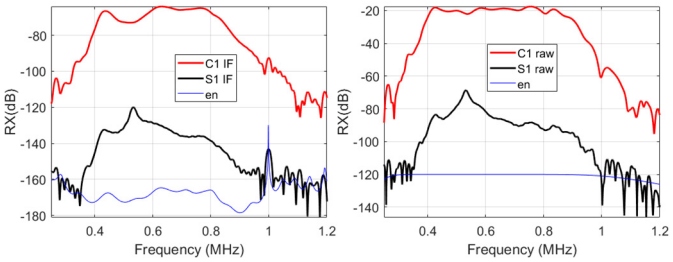

Fig. 12. Calibration and sample signals spectra in case of 20 μs long APWP excitation with spectral losses compensated: after PuC using IF (left) and raw signal (right).

Two $W(\omega)$ filter types were used: 1) fourth-order Butterworth bandpass filter with lower and upper passband frequencies corresponding to LFM range, termed as IF in further analysis and 2) Wiener-like [47] filter, termed as WF in further analysis

$$W(\omega) = \bar{C}(\omega)^2 \Big/ \left(\bar{C}(\omega)^2 + \bar{N}(\omega)^2 \right) \tag{10}$$

where $\bar{C}(\omega)$ is the calibration signal, averaged in time domain and then transformed to frequency domain, $\bar{N}(\omega)$ is noise signal, power-wise averaged in frequency domain.

Refer Fig. 11 for PuC results with IF application. This time, in order to demonstrate positive effects, much longer, 350 μs long, but same 250 kHz–1.1 MHz frequency range LFM excitation signal was used.

It can be noted that no sidelobes Fig. 11 (left) are present in front, and PuC result matches the WB pulse excitation. Obtained signals correspond to excitation containing uniform spectrum, that is, wideband Dirac pulse (actually, unity pulse). One can compare Fig. 11 IF performance to Fig. 4 (right) (MF) and Fig. 5 (MMF).

Yet, there are adverse effects too. Programming of the spectral shape is no longer possible in such case. Excitation signal spectra is shaped if compensation of the spectral losses [40], [41], [42], [46] or stronger contribution of some frequency range is required. However, application of IF turns the calibration signal spectrum into system AC response. Refer Fig. 12 (left) below for calibration and sample signal spectra in case of spectral losses compensation within −20 dB bandwidth (refer Fig. 2). White (AWGN) noise was used to better reflect the influence of the processing on the noise spectral density.

While raw signals have flat, as intended, spectra, PuC using IF destroys the programmed shape. It can be noted that

SNR remains the same, note noise spectral density plot for compressed and raw data ("en" label, blue curve). If fitting is done in time domain, more stress will be on transmission peak frequencies, but not where compensation was intended (below 0.4 MHz and beyond 0.8 MHz).

D. Solution for Preserving the Spectra: Decompression

Compressed signal can be gated if calibration and sample signal ringdown is sufficiently damped at the overlapping reflections position. Calibration signal is very short [refer Fig. 2 (left)], besides, interfering reflection for this signal is twice further. Sample signal [refer Fig. 6 (left)] is sufficiently damped at 180 μs, and, if correlation sidelobes are not present, can be gated.

Then, after gating the signal, it is decompressed back using the inverse of used processing, for example, for IF it is

$$C_{\mathrm{IFd}}(\omega) = C_{\mathrm{IF}}(\omega)\, G(\omega)$$
$$S_{\mathrm{IFd}}(\omega) = S_{\mathrm{IF}}(\omega)\, G(\omega). \tag{11}$$

Filter $W(\omega)$ used in (9) in such case is not essential, because noise gain [due to division by $G(\omega)$] in low-SNR regions, produced by (9) is removed by multiplication by $G(\omega)$ in (11).

III. Performance Evaluation

Performance evaluation was carried out with same setup described earlier. NC-RUS measurements of 2 mm thick polycarbonate plate were carried out using two air-coupled 20 mm diameter, and 650 kHz center frequency transducers [43], spaced 34 mm apart. Three different sets of signals were used: 1) LFM signals, covering 250 kHz–1.1 MHz range; 2) APWP signals, optimized to make flat received signal spectrum at −20 dB passband (380–900 kHz); and 3) APWP signals, optimized to match the transducer AC response within −20 dB passband (380–900 kHz). Several durations were used: 10, 20, 50, 100, 200, and 350 μs (limited by acquisition system capabilities). Excitation for Calibration measurement used 7 V, Sample measurement used 10, 20, and 50 V amplitudes. Received signals were amplified using digitally programmable gain preamplifier with 0.1–3 MHz passband. Calibration signal used 16 dB gain, gain for Sample signal varied from 57 dB (50 V excitation) to 62 dB (10 V excitation). Signals were collected using 10-bit 12.5 MHz sampling frequency ADC. Ambient conditions were relative humidity 40%, temperature 27.7 °C, and pressure 101.8 kPa.

Simulation used 18-th order IIR filter, derived from LFM measurements to simulate the calibration signal. Equation (3) was used to simulate the sample signal, using $h = 2$ mm, $c_s = 2220$ m/s, $n = 1, \rho_s = 1200$ kg/m^3, and $\alpha_0 = 45$ Np/m @ 650 kHz). Noise was colored, using previously measured noise spectral density at system input.

Ten PuC types were investigated: 1) raw signal (label "Raw"); 2) PuC using IF (label "IF"); 3) PuC using MF (label "MF"); 4) PuC using MMF (label "MMF"); 5) PuC using WF (label "WF"); 6) raw signal with interfering reflections reduced (label "Ungated"); 7) PuC using IF with following decompression (label "IFd"); 8) PuC using MF with following decompression (label "MFd"); 9) PuC using MMF with following decompression (label "MMFd"); and 10) PuC using WF with following decompression (label "WFd"). Processing 6) used compressed IF signal, where first reflection was gated out, decompressed, and resulting signal subtracted from raw signal. Such processing resulted in the removal of the interfering reflections and gating for was not required (label "Ungated").

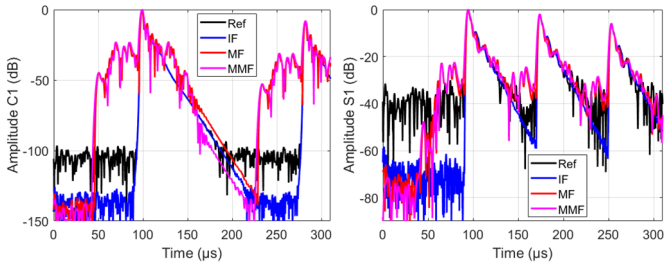

Fig. 13. Hilbert envelope of compressed calibration (left) and sample (right) signals in case of 50 μs long LFM excitation.

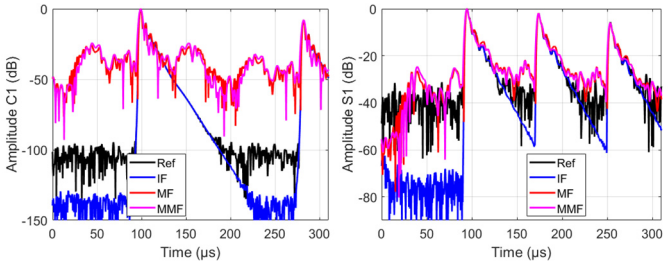

Fig. 14. Hilbert envelope of compressed calibration (left) and sample (right) signals in case of 100 μs long LFM excitation.

In simulation and real experiments, 100 measurements were taken with each excitation signal set which were processed by 10 PuC types and then submitted for NC_RUS fitting in order to estimate the sample parameters (height h, velocity c_s, density ρ_s, and acoustic attenuation α_0). Obtained results were statistically processed to obtain the bias and random errors.

In simulation, bias errors were calculated by taking the absolute difference between the sample parameters and mean values estimated by NC-RUS. In experiments, bias errors were calculated by taking the absolute difference between the sample parameters estimated using "Ungated" signals and mean values estimated by NC-RUS.

A. Simulation Results

Advantage of IF PuC can be seen from Figs. 13–15. Hilbert envelope of the compressed signal was taken and presented in logarithmic range. Signal labeled "Ref" is a unity pulse.

In order to improve SNR and expose the sidelobes, highest (50 V) excitation was used and 100 waveforms averaged.

Fig. 13 is representing the case when overlapping with interfering reflection is less pronounced (see Fig. 10), because 50 μs long LFM excitation was used. It can be noted that interfering sidelobes span approximately 50 μs, corresponding to the duration of excitation chirp. Adverse effects of interfering sidelobes can be noted in Fig. 13 (right): approximately half of the sample reverberation ringdown tail is corrupted by MF correlation sidelobes.

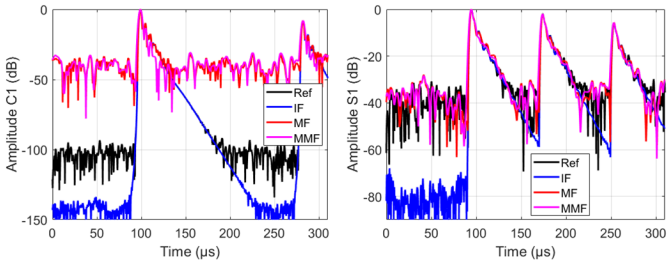

Fig. 15. Hilbert envelope of compressed calibration (left) and sample (right) signals in case of 350 μs long LFM excitation.

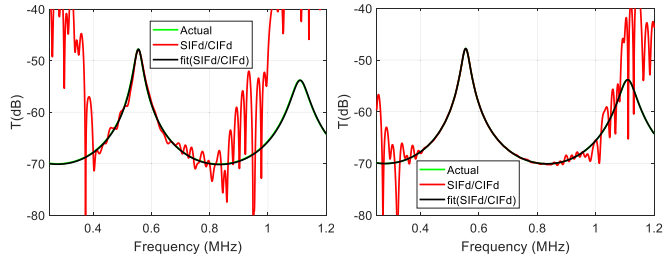

Fig. 16. Sample transmission AC response for lowest SNR (left, 10 μs 10 V LFM) and highest SNR (right, 350 μs 50 V LFM).

Fig. 14 is representing the case when overlapping with interfering reflection is more pronounced, because 100 μs long LFM excitation was used. In this case whole ringdown tail is corrupted by MF correlation sidelobes.

Interference is even more severe for Fig. 15 case: now sidelobes of first, second, and third interfering reflection are interfering with sample reverberation ringdown tail.

It can be noted that MF produces lower than IF noise floor (region 0–50 μs in Fig. 13). Yet, adverse effects of MF and MMF correlation sidelobes are much higher than noise floor. In addition, sidelobes are most pronounced in a region of interest (100–150 μs) on which NC-RUS fitting is performed. While in Fig. 13 (50 μs long LFM) sidelobes cover just 50 μs, in case of 100 μs (Fig. 14), or 350 μs (Fig. 15) long excitation signal the sidelobes are covering all ringdown tail of signal, objecting proper gating and NC-RUS processing.

Fig. 16 is to demonstrate the difference between lowest SNR (left, 10 μs 10 V LFM) and highest SNR (right, 350 μs 50 V LFM) sample transmission.

Plots include measured transmission, obtained by IF compression-decompression (label "SIFd/CIFd"), actual transmission response used for simulation (label "Actual") and NC-RUS fitting result (label "fit(SIFd/CIFd)"). Last two curves ("Actual" and "fit(SIFd/CIFd)") completely cover each other.

It can be noted that only peak at 550 kHz has reasonable SNR in case of 10 μs 10 V LFM, meanwhile 350 μs 50 V LFM is producing high SNR even for valley at 850 kHz. Fitting performance at low SNR (refer to whisker plots in Fig. 17) is similar for all PuC types and comparison is complicated. Whisker plots contain two horizontal lines. One is based on actual value used in simulation (label "Expected"), another is a mean value of uncompressed signal (label "Mean (raw)"). Uncompressed signal can be used because duration of LFM chirp is 10 μs, so there is no overlap from interfering

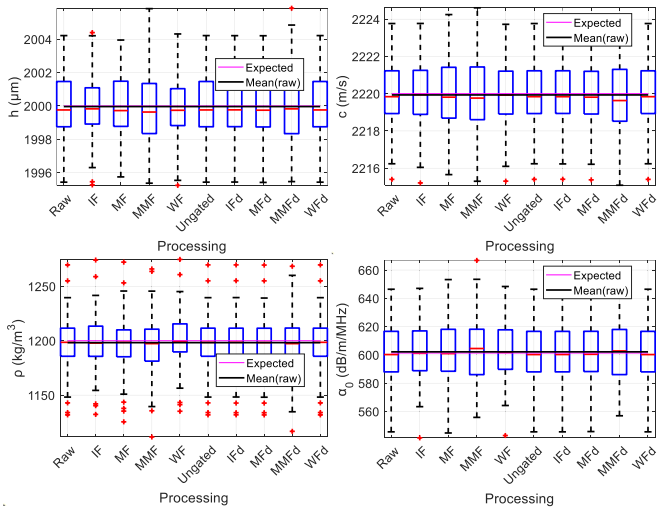

Fig. 17. NC-RUS results at lowest SNR (10 μs 10 V LFM).

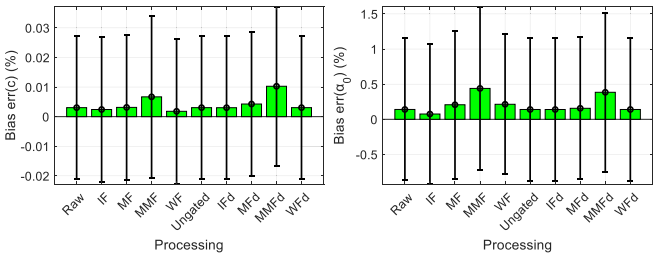

Fig. 18. Bias errors at lowest SNR (10 μs 10 V LFM): sample velocity (left) and attenuation (right).

reflection. However, it can be already noted that bias errors are higher for MF, MMF, and MMFd PuC. Raw and ungated case are at the same errors level as IF, because LFM signal duration is short and no overlapping occurs.

Bias error can be estimated, by comparing the mean of NC-RUS measurements (100 measurements were taken) and actual value used in simulation. Yet, as can be seen from Fig. 17, bias errors are much smaller than random errors caused by noise. In further analysis, bias error plots were augmented by adding whiskers indicating an expected range after averaging 100 measurements. Bias errors are presented in Fig. 18. Only velocity and attenuation errors are plotted.

It can be noted that velocity errors are already low. The reason is that thickness and velocity are mainly estimated from time delay measurements and delay-based measurements are always producing lower errors. Meanwhile, attenuation estimation is based on amplitude; therefore, errors are larger. It can be noted that that MF performance is comparable to IF at low SNR, because adverse effects of the sidelobes are masked by high noise floor.

It can be seen that mean is not estimated reliably: expected variation (black whiskers) of mean is larger than bias error itself. Situation is already improved at 10 V and 100 μs (refer Fig. 19 for bias errors obtained in NC-RUS measurements), because SNR is improved due to longer excitation signal. At 100 μs there is an overlap of sidelobes and performance of Raw, MF, MMF, MFd, and MMFd suffers. Same can be noted: errors are smaller for delay-based measurements (thickness

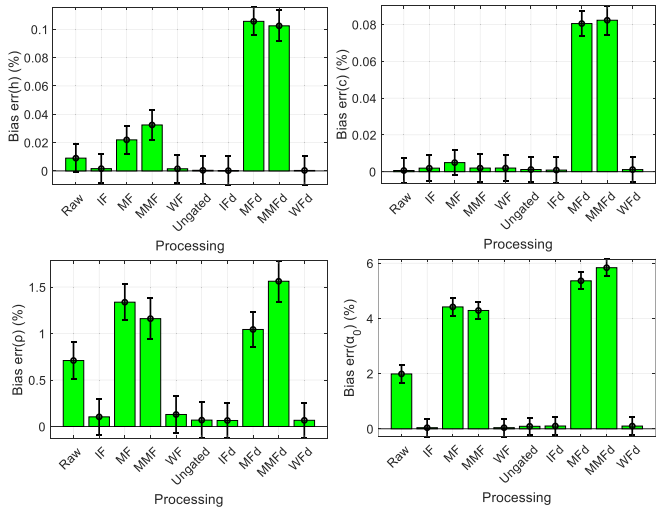

Fig. 19. Bias errors at moderate SNR, 100 μs 10 V LFM.

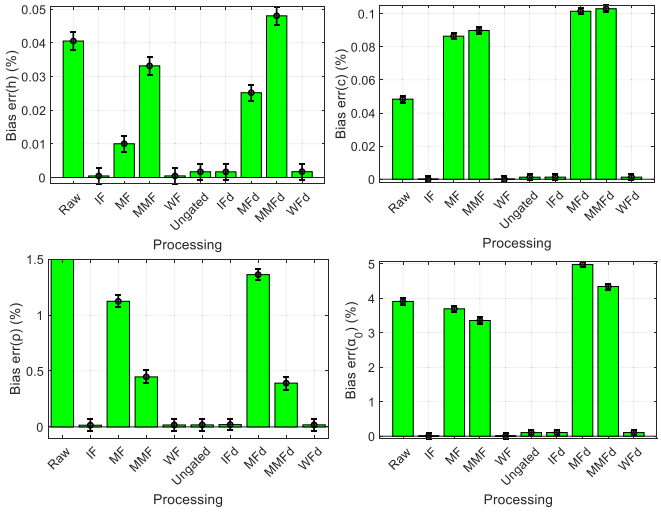

Fig. 20. Bias errors at high SNR, 350 μs 20 V LFM.

and velocity), while amplitude-based measurements (density and attenuation) have higher errors.

At 10 V and 350 μs (refer Fig. 20) overlap of sidelobes is significant and performance of Raw, MF, MMF, MFd, and MMFd suffers. Errors for IF, WF, IFd, and WFd are very low.

Essential conclusion can be drawn from Figs. 19 and 20: sidelobes, that are present in MF or MMF compressed signals, produce bias errors. It is interesting to point out that bias errors for MF and MMF were lower (0.2%–0.45% for attenuation, 0.2%–0.3% for density) for shorter (10 μs) excitation because there was no overlapping, but were overwhelmed by random errors. As soon as excitation signal got longer (100–350 μs), random errors went down, but bias errors for MF and MMF grow significantly (3.4%–6% for attenuation, 0.5%–1.4% for density). Meanwhile, IF and WF performance is much better and improves with longer excitation. For 10 μs excitation bias errors are 0.1%–0.2% for attenuation and 0.1%–0.2% for density, longer excitation results in 0.08%–0.1% for attenuation and 0.015%–0.02% for density.

Long sequences, especially at high excitation voltage, have extra SNR margin in passband; therefore, spectrum

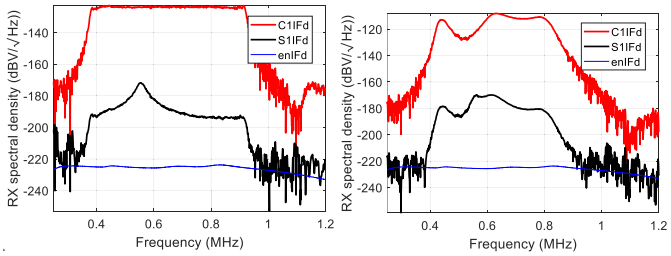

Fig. 21. Calibration and sample spectra in case of losses compensation (left) and transmission match (right). 50 V 350 μs long APWP sequence.

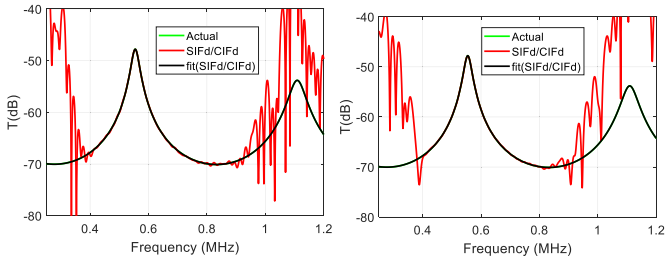

Fig. 22. Sample transmission AC response in case of losses compensation (left) and transmission match (right). 50 V 350 μs long APWP sequence.

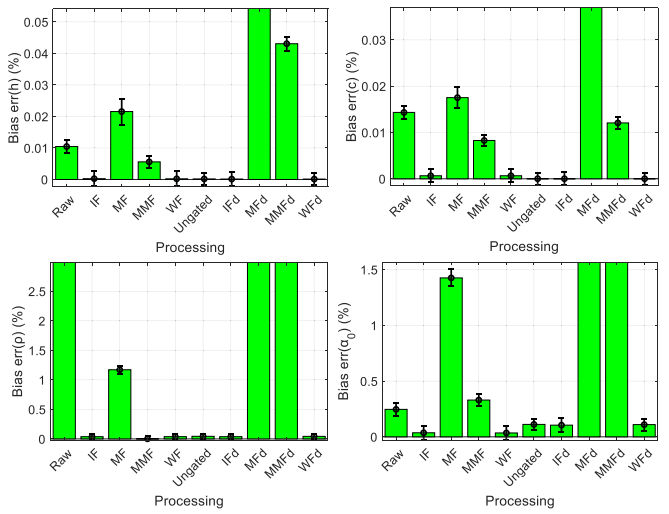

Fig. 23. NC-RUS bias errors in case of losses compensation.

programming can be used to improve the SNR in regions where it is low by using APWP excitation with losses compensation [Figs. 21 (left) and 22 (left)]. Alternatively, excitation can be programmed to concentrate in regions of good sensitivity, that is, matched to system transmission [Figs. 21 (right) and 22 (right)]. Both cases use same length, 350 μs 50 V APWP sequence, only spectral content is different.

NC-RUS bias errors for 350 μs 50 V APWP with losses compensation are presented in Fig. 23.

Same can be concluded from Fig. 23 results: performance of Raw, MF, MMF, MFd, and MMFd is unacceptable: bias error for density for MFd is 28%, 7% for MMFd, α_0 is estimated with 14% bias for MFd, 6% for MMFd. No significant improvement can be noted on IF or WF results in comparison to Fig. 20 where no compensation was used. The only results

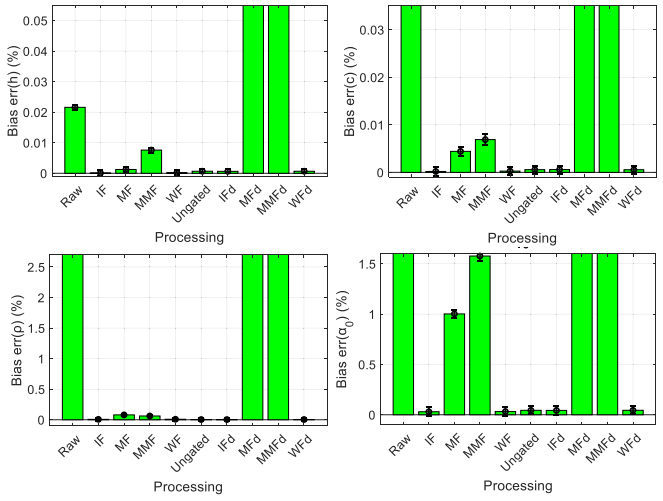

Fig. 24. NC-RUS bias errors with transmission-matched spectrum excitation.

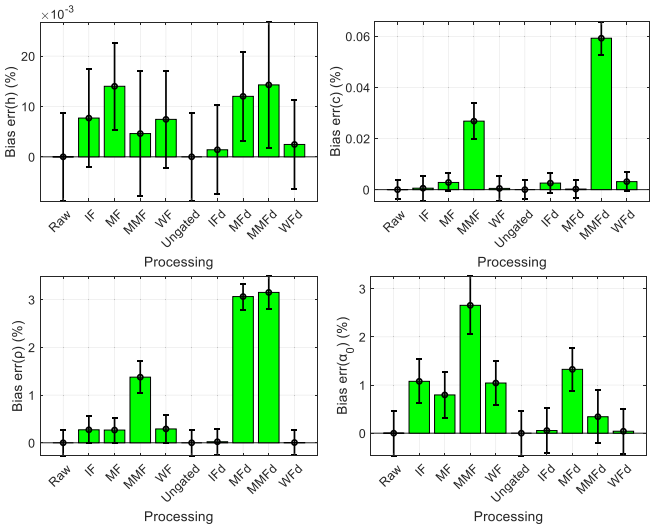

Fig. 25. NC-RUS bias errors at 10 μs 20 V LFM excitation.

that improved were velocity and thickness: bias error was reduced from 0.002% to 0.001% in case of IFd and WFd processing.

NC-RUS results for 50 V 350 μs APWP with transmission-matched spectrum are presented in Fig. 24.

In case of transmission-matched spectrum, performance of Raw, MF, MMF, MFd, and MMFd is low: bias error for density for MFd is 182%, 25% for MMFd, α_0 is estimated with 43% bias for MFd, 3% for MMFd. It can be noted that thickness and velocity estimation errors are very low. The reason is that that these parameters are mainly estimated from delay, and delay-based measurements always have lower errors. Yet, compared to losses-compensated case, there was a performance reduction for velocity and thickness: bias error increased form 0.001% in case of loss compensation to 0.004% in case of IFd and WFd processing.

It can be concluded that both compressed and decompressed IF and WF PuC performs the best. Ungated measurement has equal to IF performance; therefore, can be used as ground truth in real experiments.

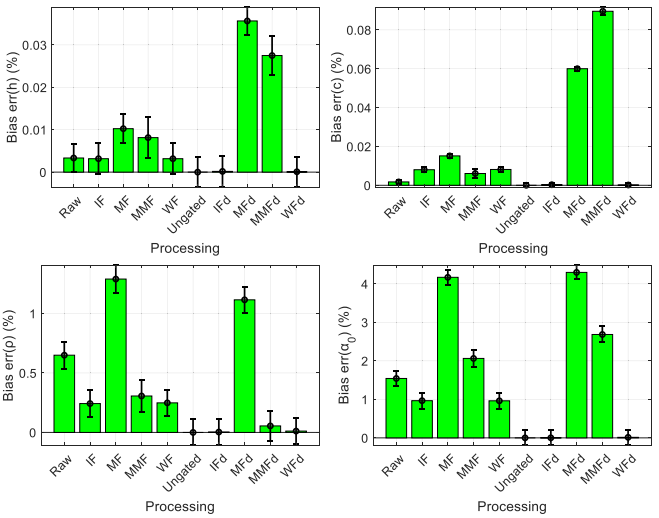

Fig. 26. NC-RUS bias errors at 100 μs 20 V LFM excitation.

B. Experimental Results

Several measures were taken to reduce the bias errors in experimental measurements. Temperature drift was compensated using technique [48]. Excitation voltage was measured using dedicated ADC. Preamplifier gain was calibrated. However, bias errors to evaluate are very small. Therefore, it was decided to use the "Ungated" measurement results as reference for sample parameters.

Bias errors of NC-RUS sample parameters measurement for 10 μs 20 V LFM excitation are presented in Fig. 25. No overlapping was expected (but low SNR), yet, performance of MF, MMF, MFd, and MMFd was the lowest. This can be attributed to signal distortion: Raw and Ungated have lowest errors because no compression is used. As expected, IF and WF have larger errors for parameters which estimation is mainly based on amplitude (density and attenuation). IFd and WFd performance is the best.

Bias errors in case of 100 μs 20 V LFM (Fig. 26) and 350 μs 20 V LFM (Fig. 27) are lowest for IFd and WFd. Both cases will have sidelobes that overlap with main signal.

It can be noted that in case of sidelobes overlapping bias errors of MF, MMF, MFd, and MMFd PuC increase compared to IF or WF compression. While sample thickness error is 0.003% at 100 μs and 0.007% at 350 μs for IF and WF, 0.0002%–0.0005% for IFd and WFd, MF, and MMF compression produces 0.01% at 100 μs and 0.07% at 350 μs. Thickness estimation errors are up to 350 times larger for MF than IF. Sample velocity estimation errors are up to 200 times larger for MFd than IFd. Density estimation bias errors are 0.24%–0.25% for IF and WF, 0.003%–0.008% for IFd and WFd, but 1.3%–2.4% for MF and MMF% or even 4.9% for MMFd. Density estimation bias errors are up to 1600 times larger for MF than IF. Sample attenuation estimation bias errors are up to 700 times larger for MFd than IFd. Bias errors of MF,

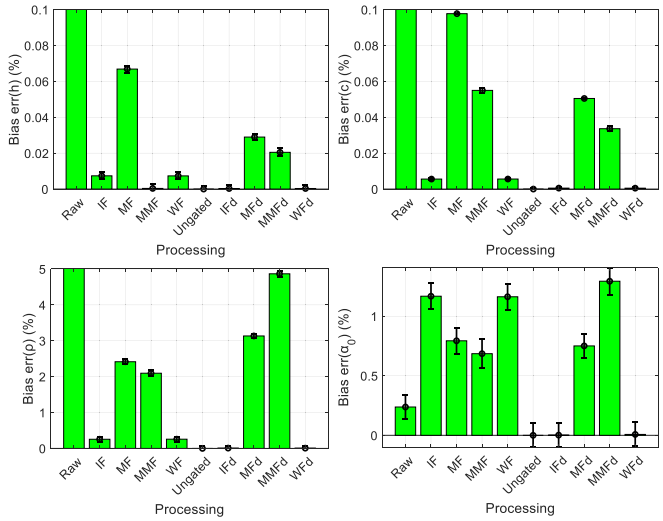

Fig. 27. NC-RUS bias errors at 350 μs 20 V LFM excitation.

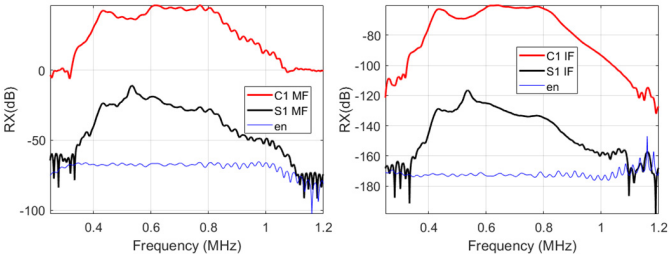

Fig. 28. Calibration and sample spectra in case of MF (left) and IF (right) PuC. 10 V 50 μs long LFM chirp.

MMF, MFd, and MMFd PuC increase with longer excitation signals.

IV. Discussion

Explanation of better IF performance compared to MF can be seen from resulting signals spectra, presented in Fig. 28.

While MF-compressed signals contain Fresnel ripples, imposed by LFM chirp spectrum, IF-compressed signals do not have these ripples. Equations (1)–(9) can be rewritten as

$$C_{\mathrm{MF}}(\omega) = C(\omega)\,|G(\omega)|/\angle G(\omega)$$
$$C_{\mathrm{IF}}(\omega) = C(\omega)/\left(|G(\omega)|\,\angle G(\omega)\right). \tag{12}$$

Noting, that

$$\mathrm{C}(\omega) = |G(\omega)|\,\angle G(\omega)\,T_{\mathrm{sys}}(\omega) \tag{13}$$

where T_{sys} is a system (transmitting transducer, air propagation, receiving transducer, amplifiers, and filters) transmission response. This results in

$$C_{\mathrm{MF}}(\omega) = T_{\mathrm{sys}}(\omega)\,|G(\omega)|^2$$
$$C_{\mathrm{IF}}(\omega) = T_{\mathrm{sys}}(\omega). \tag{14}$$

Now essential difference can be seen: IF produces pure system response, as if excitation was carried out using delta pulse. Equations above omitted filter $W(\omega)$, used in IF which is optional, intended for noise reduction in low-SNR regions. If filter is broadband enough not to affect the LFM spectrum, (14) is still valid.

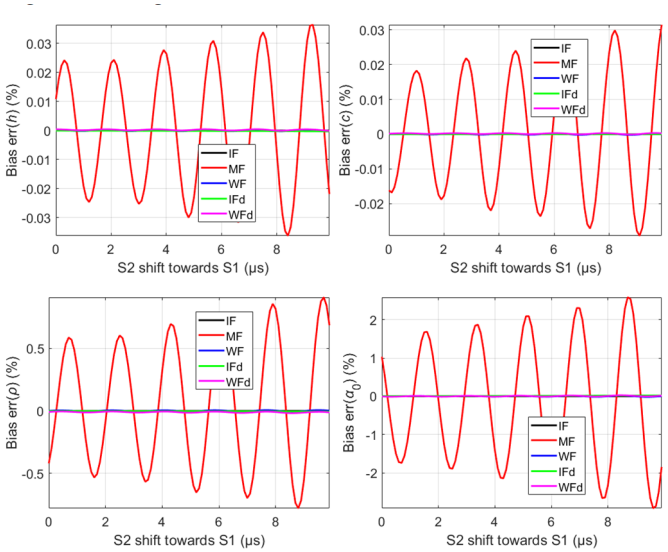

Fig. 29. NC-RUS bias errors variation with interfering reflection position shift left at 50 μs LFM excitation.

Yet, such large difference in NC-RUS sample parameters estimation errors between MF and IF PuC sounds unusual. According to Figs. 10 and 14, sidelobes are quite low, −30 to 40 dB. The essence lies in thickness resonance evaluation, used in NC-RUS. Note the signal ringdown in Fig. 7 which is caused by reverberation in sample. This sample reverberation carries essential information about the sample impedance and attenuation. If sidelobes of the interfering reflection overlap with this ringdown, this is equivalent to change in sample impedance and attenuation. Moreover, since this part of signal is decaying, even slightest change can result in significant estimation errors. Furthermore, as it was pointed out in [53], influence of interfering reflection also depends on temporal distance between analyzed and interfering signal. Both amplitude and time position are affected. Therefore, it makes sense to analyze how NC-RUS errors change when distance in time of interfering reflection is varied.

Same simulation as per Section III was carried out, except that noise was not added to rectify only bias errors. Excitation used 50 μs LFM chirp. Position of interfering reflection S2 was additionally shifted left toward measurement signal S1 from 0 s (same situation as per Section III) to 10 μs with 0.1 μs step. In such cases, influence of interfering reflection is gradually increased and effect on NC-RUS bias errors can be studied (see Figs. 29 and 30).

From Fig. 29 it can be concluded that PuC using MF produce much larger errors than IF of WF compression. It can be noted that adverse effects of interference depend on spacing between measurement signal S1 and interfering reflection S2 and are increasing with spacing reduced. There are positions when bias error for one parameter is zero, but at very same offset, other parameters have large errors. For instance, at 0.75 μs offset, thickness h estimation errors are zero, but density ρ_s and attenuation α_0 errors are the largest at this offset. Maximum bias error for MF compression is 0.032% (versus $3 \cdot 10^{-6}$% for IF compression) for sample velocity and thickness. It is 1% (versus $5 \cdot 10^{-5}$% for IF compression) for

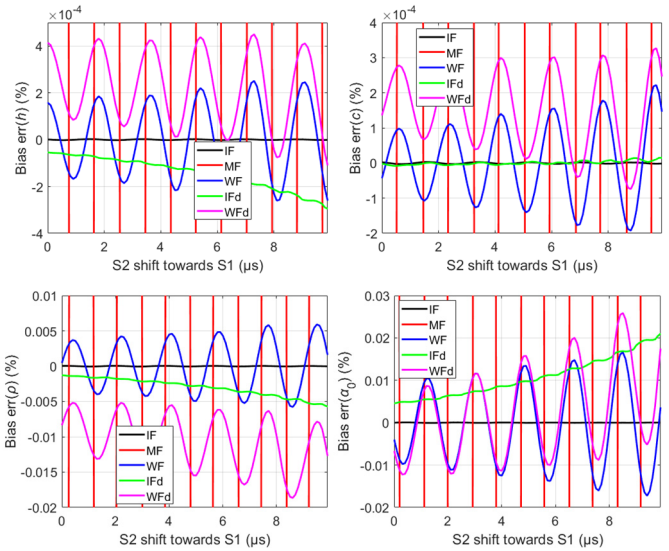

Fig. 30. Zoom-in of NC-RUS bias errors variation with interfering reflection position shift left at 50 μs LFM excitation.

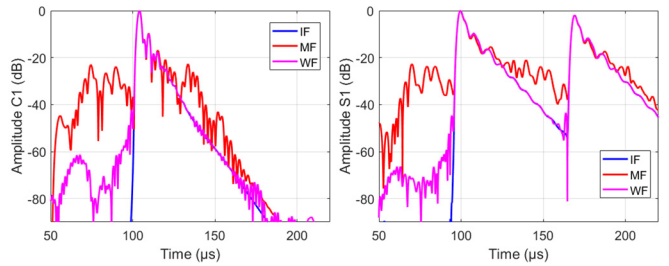

Fig. 31. Hilbert envelope of compressed calibration (left) and sample (right) signals in case of 50 μs long LFM excitation.

density and 2.7% (versus $6 \cdot 10^{-6}$% for IF compression) for sample attenuation.

Fig. 30 is a zoom-in version of Fig. 29, aimed to have a better insight into bias errors of IF, WF, IFd, and WFd compression.

It can be noted that IF, WF, IFd, and WFd compression produces much smaller errors than MF or MMF compression. Yet, now it can be noted that WF compression is producing larger errors than IF compression. Maximum bias error for WF compression is $2.3 \cdot 10^{-4}$% (versus $3 \cdot 10^{-6}$% for IF compression) for sample velocity and thickness, 0.006% (versus $5 \cdot 10^{-5}$% for IF compression) for density and 0.018% (versus $6 \cdot 10^{-6}$% for IF compression) for sample attenuation.

Analysis of calibration and sample signal envelope after IF, MF, and WF compression, presented in Fig. 31 reveals the reason: WF compression does have sidelobes.

WF is constructed in such a way that at frequencies where SNR is low, it turns into MF. This gives rise for sidelobes. Still, WF sidelobes are approximately 50 dB lower than MF.

IFd and WFd compression-gating-decompression processing have comparable performance. IFd performs slightly better than WFd, yet with additional bias, caused by sample ringdown gating.

It can be concluded that IF compression is producing best results when used in NC-RUS sample parameters estimation. Best result is achieved due to lowest compression sidelobes and fitting in time instead of frequency domain (no adverse gating effects). Still, IFd processing is the only way to maintain the spectral content provided by programmable excitation. Errors in such cases are still significantly lower than MF. Maximum bias error for IFd processing is 0.003% (versus 0.032% for MF compression) for sample velocity, $2 \cdot 10\%^{-5}$% (versus 0.032% for MF compression) for sample thickness, 0.006% (versus 1% for MF compression) for density and 0.02% (versus 2.7% for MF compression) for sample attenuation.

While presented material focuses on reducing bias errors in NC-RUS, it is worth to mention that the ideal-pulse-like response achieved via IF-based PuC is applicable to diverse applications. Applications, (ranging [25], [26], thickness [30], [32], flow [27] measurement) using the time delay estimation (TDE) in combination with coded excitation [37], [39], [40] in order to achieve high SNR would benefit. It was demonstrated [53] that delay estimate develops bias errors if neighboring signal is close. Bias error appears if neighboring signal not only has a single peak but also contains sidelobes which overlap with measured peak. IF-based PuC can reduce TDE bias errors. Imaging applications are using coded excitation for SNR and resolution improvement [31], [32]. Presence of the sidelobes reduces contrast, can result in artifacts [49], [50]. Use of long SS sequences in case of MF-based PuC only worsens the situation: span of the sidelobes is increased. Meanwhile, use of long sequences and IF-based PuC improves the SNR and reduces the sidelobes. Laser ultrasound is usually using single, high-power pulse for excitation, usually resulting in ablation regime, which damages the surface equipment is bulky and expensive. It was already demonstrated [54] that semiconductor laser diode can be used, resulting in more compact, less expensive equipment. SS excitation [55], [56] together with IF-based PuC would allow to operate in thermoelastic mode but with higher SNR and low sidelobes.

V. Conclusion

Long SS signals are demanded in NC-RUS in order to avoid distortion in air, expand the bandwidth available for analysis and achieve high SNR.

Interfering reflections between sample and transducer occur in NC-RUS measurements, which object the application of longer than 50 μs excitation (if distance between transducers is 34 mm). If would be natural to expect that SS signals can be compressed using MF. However, it was demonstrated that pulse compression using MF produces correlation sidelobes. Simulation and experiment results indicate that these sidelobes produce bias errors in NC-RUS measurements which increase with excitation signal length.

Solution proposed uses IF with NC-RUS fitting in time domain. Result of such compression is as if excitation with ideal delta pulse was used, but with significantly increased SNR. IF is effective because it removes Fresnel ripples, imposed by LFM chirp. Fitting in time domain is removing the adverse effects of signal gating, required for frequency domain fitting.

Significant NC-RUS bias errors reduction is achieved if MF is replaced by IF. Maximum bias error for MF compression is

0.032% (versus $3 \cdot 10^{-6}$% for IF compression, 1000 times reduction) for sample velocity and thickness, 1% (versus $5 \cdot 10^{-5}$% for IF compression, 20 000 times reduction) for density and 2.7% (versus $6 \cdot 10^{-6}$% for IF compression, 450 000 times reduction) for sample attenuation.

Yet, such compression removes the spectral content effects, produced by excitation signal. This could be of some significance if spectral losses compensation is aimed by using programmable spectral content excitation.

Solution was proposed for such case. It uses IF, then compressed signal is gated and decompressed. In such cases, adverse effects of gating cannot be avoided if sample reverberation time is longer than distance to nearest interfering reflection. Still, errors are much smaller than in case of MF compression. Maximum bias error for such processing is 0.003% (versus 0.032% for MF compression, a tenfold reduction) for sample velocity, $2 \cdot 10^{-5}$% (versus 0.032% for MF compression, 1600 times reduction) for sample thickness, 0.006% (versus 1% for MF compression, 160 times reduction) for density and 0.02% (versus 2.7% for MF compression, 130 times reduction) for sample attenuation.

REFERENCES

[1] H. Zhang, Z. Zong, X. Rui, and S. Liu, "A linear mapping dispersion compensation method for debonding detection of honeycomb sandwich structure based on air-coupled ultrasound," *IEEE Trans. Instrum. Meas.*, vol. 74, pp. 1–10, 2025, doi: 10.1109/TIM.2025.3534226.

[2] P. O. Moore, *Nondestructive Testing Handbook*, vol. 10, 3rd ed., Columbus, OH, USA: American Society for Nondestructive Testing, 2012.

[3] Y. Cheng, G. Xia, R. Zhang, Y. Zhang, Y. Li, and J. Huang, "A novel air-coupled ultrasonic technique for assessing the weathering degree of sandstone heritage," *J. Cultural Heritage*, vol. 74, pp. 204–213, Jul. 2025.

[4] I. Solodov, K. Pfleiderer, H. Gerhard, S. Predak, and G. Busse, "New opportunities for NDE with air-coupled ultrasound," *NDT E Int.*, vol. 39, no. 3, pp. 176–183, Apr. 2006, doi: 10.1016/j.ndteint.2005.07.002.

[5] H. Mortada, S. El Mousharrafie, E. Mahfoud, and M. Harb, "Noncontact nondestructive ultrasonic techniques for manufacturing defects monitoring in composites: A review," *Structural Health Monitor.*, vol. 23, no. 3, pp. 1969–1997, May 2024, doi: 10.1177/14759217231184589.

[6] Y. Fang, L. Lin, H. Feng, Z. Lu, and G. W. Emms, "Review of the use of air-coupled ultrasonic technologies for nondestructive testing of wood and wood products," *Comput. Electron. Agricult.*, vol. 137, pp. 79–87, May 2017, doi: 10.1016/j.compag.2017.03.015.

[7] D. E. Chimenti, "Review of air-coupled ultrasonic materials characterization," *Ultrasonics*, vol. 54, no. 7, pp. 1804–1816, Sep. 2014, doi: 10.1016/j.ultras.2014.02.006.

[8] A. Sampaleanu, P. Zhang, A. Kshirsagar, W. Moussa, and R. J. Zemp, "Top-orthogonal-to-bottom-electrode (TOBE) CMUT arrays for 3-D ultrasound imaging," *IEEE Trans. Ultrason., Ferroelectr., Freq. Control*, vol. 61, no. 2, pp. 266–276, Feb. 2014, doi: 10.1109/TUFFC.2014.6722612.

[9] W. Essig et al., "Air-coupled ultrasound–emerging NDT method," *ZfP-Zeitung*, vol. 173, pp. 32–43, Feb. 2021. [Online]. Available: https://www.dgzfp.de/wp-content/uploads/2025/03/Zeitung173.pdf

[10] T. Pernu, J. Saarilahti, and T. Sillanpää, "Real-time frequency matching circuit for a high sensitivity cMUT-based gas flow sensor," *Sens. Actuators A, Phys.*, vol. 383, Mar. 2025, Art. no. 116252, doi: 10.1016/j.sna.2025.116252.

[11] A. Giacomozzi, J. Benedito, T. E. G. Álvarez-Arenas, and J. V. García-Perez, "Air-coupled ultrasonic inspection of foods: A review," *IEEE Open J. Ultrason., Ferroelectr., Freq. Control*, vol. 4, pp. 100–115, 2024, doi: 10.1109/OJUFFC.2024.3457503.

[12] L. Fariñas, D. Sancho-Knapik, J. J. Peguero-Pina, E. Gil-Pelegrín, and T. E. G. Álvarez-Arenas, "Origin, development, and applications of air-coupled broadband ultrasounds for the study of tissues and water relations in plant leaves: A review," *IEEE Open J. Ultrason., Ferroelectr., Freq. Control*, vol. 4, pp. 77–88, 2024, doi: 10.1109/OJUFFC.2024.3433316.

[13] V. T. Rathod, "A review of acoustic impedance matching techniques for piezoelectric sensors and transducers," *Sensors*, vol. 20, no. 14, p. 4051, Jul. 2020, doi: 10.3390/s20144051.

[14] T. E. G. Alvarez-Arenas, "Acoustic impedance matching of piezoelectric transducers to the air," *IEEE Trans. Ultrason., Ferroelectr., Freq. Control*, vol. 51, no. 5, pp. 624–633, May 2004, doi: 10.1109/TUFFC.2004.1320834.

[15] J. Gu, Q. Zhao, B. Yin, H. Zhou, and S. Qu, "Lowering the sound transmission loss of impedance-matching structures: Data-driven optimization assisted with a priori knowledge," *Mater. Design*, vol. 232, Aug. 2023, Art. no. 112091, doi: 10.1016/j.matdes.2023.112091.

[16] T. Gudra and K. J. Opielinski, "Influence of acoustic impedance of multilayer acoustic systems on the transfer function of ultrasonic airborne transducers," *Ultrasonics*, vol. 40, nos. 1–8, pp. 457–463, May 2002, doi: 10.1016/s0041-624x(02)00159-2.

[17] L. M. Brekhovskikh and O. A. Godin, *Acoustics of Layered Media I. Plane and Quasi-Plane Waves*. Berlin, Germany: Springer, 1990.

[18] H. E. Bass, L. C. Sutherland, A. J. Zuckerwar, D. T. Blackstock, and D. M. Hester, "Atmospheric absorption of sound: Further developments," *J. Acoust. Soc. Amer.*, vol. 97, no. 1, pp. 680–683, Jan. 1995.

[19] Calculation of the Absorption of Sound By the Atmosphere, Standard ISO 9613-1, 1996.

[20] E. Blomme, D. Bulcaen, and F. Declercq, "Air-coupled ultrasonic NDE: Experiments in the frequency range 750 kHz–2MHz," *NDT E Int.*, vol. 35, no. 7, pp. 417–426, Oct. 2002, doi: 10.1016/s0963-8695(02)00012-9.

[21] T. G. Álvarez-Arenas and L. Díez, "Novel impedance matching materials and strategies for air-coupled piezoelectric transducers," in *Proc. IEEE Sensors*, Nov. 2013, pp. 1494–1497.

[22] L. Amoroso et al., "Novel nanocomposite materials for improving passive layers in air-coupled ultrasonic transducer applications," in *Proc. IEEE IUS*, Oct. 2019, pp. 2608–2611, doi: 10.1109/ULTSYM.2019.8925712.

[23] C. Ferraro et al., "Light and strong SiC networks," *Adv. Funct. Mater.*, vol. 26, no. 10, pp. 1636–1645, Mar. 2016, doi: 10.1002/adfm.201504051.

[24] H. Tanaka, S. Machida, and M. Nanri, "Active acoustic impedance matching using CMUT structure," in *Proc. IEEE Int. Ultrason. Symp. (IUS)*, Sep. 2021, pp. 1–4, doi: 10.1109/IUS52206.2021.9593796.

[25] R. Kazys, L. Mazeika, R. Sliteris, and A. Voleisis, "Online profiling of nonplanar objects by high-resolution air-coupled ultrasonic distance measurements," *IEEE Trans. Instrum. Meas.*, vol. 56, no. 5, pp. 1825–1830, Oct. 2007, doi: 10.1109/TIM.2007.903627.

[26] M. M. Saad, C. J. Bleakley, and S. Dobson, "Robust high-accuracy ultrasonic range measurement system," *IEEE Trans. Instrum. Meas.*, vol. 60, no. 10, pp. 3334–3341, Oct. 2011, doi: 10.1109/TIM.2011.2128950.

[27] Q.-H. Meng, S.-Y. Lan, Z.-J. Yao, and G.-W. Li, "Real-time noncrosstalk sonar system by short optimized pulse-position modulation sequences," *IEEE Trans. Instrum. Meas.*, vol. 58, no. 10, pp. 3442–3449, Oct. 2009, doi: 10.1109/TIM.2009.2017663.

[28] H. Yu, C. Tan, and F. Dong, "Particle size characterization in liquid–solid dispersion with aggregates by broadband ultrasound attenuation," *IEEE Trans. Instrum. Meas.*, vol. 70, pp. 1–11, 2021, doi: 10.1109/TIM.2021.3063185.

[29] D. Hutchins, P. Burrascano, L. Davis, S. Laureti, and M. Ricci, "Coded waveforms for optimised air-coupled ultrasonic nondestructive evaluation," *Ultrasonics*, vol. 54, no. 7, pp. 1745–1759, Sep. 2014, doi: 10.1016/j.ultras.2014.03.007.

[30] S. Laureti et al., "Delamination detection in polymeric ablative materials using pulse-compression thermography and air-coupled ultrasound," *Sensors*, vol. 19, no. 9, p. 2198, May 2019, doi: 10.3390/s19092198.

[31] T. Misaridis and J. A. Jensen, "Use of modulated excitation signals in medical ultrasound. Part II: Design and performance for medical imaging applications," *IEEE Trans. Ultrason., Ferroelectr., Freq. Control*, vol. 52, no. 2, pp. 192–207, Feb. 2005, doi: 10.1109/TUFFC.2005.1406546.

[32] P. Burrascano, S. Laureti, L. Senni, and M. Ricci, "Pulse compression in nondestructive testing applications: Reduction of near sidelobes exploiting reactance transformation," *IEEE Trans. Circuits Syst. I, Reg. Papers*, vol. 66, no. 5, pp. 1886–1896, May 2019, doi: 10.1109/TCSI.2018.2862868.

[33] J. Rus and C. U. Grosse, "Thickness measurement via local ultrasonic resonance spectroscopy," *Ultrasonics*, vol. 109, Jan. 2021, Art. no. 106261, doi: 10.1016/j.ultras.2020.106261.

[34] T. E. G. Álvarez-Arenas, "Simultaneous determination of the ultrasound velocity and the thickness of solid plates from the analysis of thickness resonances using air-coupled ultrasound," *Ultrasonics*, vol. 50, no. 2, pp. 104–109, Feb. 2010.

[35] T. E. Gómez Álvarez-Arenas and D. A. Soto, "Characterization of mineral paper by air-coupled ultrasonic spectroscopy," *Ultrasonics*, vol. 52, no. 6, pp. 794–801, Aug. 2012, doi: 10.1016/j.ultras.2012.02.012.

[36] T. E. Gómez Álvarez-Arenas, M. D. Fariñas, and A. Ginel, "Fast and non-destructive ultrasonic test for face masks," *Ultrasonics*, vol. 117, Dec. 2021, Art. no. 106556, doi: 10.1016/j.ultras.2021.106556.

[37] R. Toh and S. Motooka, "Target ranging using ultrasonic sensitivity-compensated signal and pulse compression," *Japanese J. Appl. Phys.*, vol. 48, no. 7, Jul. 2009, Art. no. 07GB09, doi: 10.1143/jjap.48.07gb09.

[38] M. Pollakowski, H. Ermert, L. V. Bernus, and T. Schmeidl, "The optimum bandwidth of chirp signals in ultrasonic applications," *Ultrasonics*, vol. 31, no. 6, pp. 417–420, Nov. 1993, doi: 10.1016/0041-624x(93)90049-6.

[39] T. M. Dantas, R. P. B. Costa-Felix, and J. C. Machado, "Nonlinear frequency modulated excitation signal and modified compressing filter for improved range resolution and side lobe level of ultrasound echoes," *Appl. Acoust.*, vol. 130, pp. 238–246, Jan. 2018, doi: 10.1016/j.apacoust.2017.10.008.

[40] L. Svilainis and A. Aleksandrovas, "Application of arbitrary pulse width and position trains for the correlation sidelobes reduction for narrowband transducers," *Ultrasonics*, vol. 53, no. 7, pp. 1344–1348, Sep. 2013, doi: 10.1016/j.ultras.2013.04.001.

[41] L. Svilainis, A. Rodriguez-Martinez, A. Chaziachmetovas, and A. Aleksandrovas, "Ultrasound transmission spectral compensation using arbitrary position and width pulse sets," *IEEE Trans. Instrum. Meas.*, vol. 67, no. 8, pp. 1778–1785, Aug. 2018, doi: 10.1109/TIM.2018.2809838.

[42] M. Tayyib and L. Svilainis, "SNR equalization in non-contact resonant ultrasound spectroscopy measurements," *NDT E Int.*, vol. 154, Sep. 2025, Art. no. 103386, doi: 10.1016/j.ndteint.2025.103386.

[43] T. Gómez Alvarez-Arenas, "Air-coupled piezoelectric transducers with active polypropylene foam matching layers," *Sensors*, vol. 13, no. 5, pp. 5996–6013, May 2013, doi: 10.3390/s130505996.

[44] L. Svilainis, V. Dumbrava, and D. Kybartas, "Evaluation of the ultrasonic preamplifier noise voltage density," *J. Circuits Syst. Comput.*, vol. 23, no. 1, Jan. 2014, Art. no. 1450007, doi: 10.1142/S0218126614500078.

[45] L. Fariñas and T. E. G. Álvarez-Arenas, "Ultrasonic non-linear harmonic generation in air for the characterization of thin membranes over an ultra-wide frequency range," *Ultrasonics*, vol. 155, Nov. 2025, Art. no. 107735, doi: 10.1016/j.ultras.2025.107735.

[46] D. A. Kiefer, M. Fink, and S. J. Rupitsch, "Simultaneous ultrasonic measurement of thickness and speed of sound in elastic plates using coded excitation signals," *IEEE Trans. Ultrason., Ferroelectr., Freq. Control*, vol. 64, no. 11, pp. 1744–1757, Nov. 2017, doi: 10.1109/TUFFC.2017.2746900.

[47] W. H. Press, S. A. Teukolsky, W. T. Vetterling, and B. P. Flannery, *Numerical Recipes: The Art of Scientific Computing*. Cambridge, U.K.: Cambridge Univ. Press, 2007, pp. 649–652.

[48] Z. Nakutis, P. Kaskonas, D. Liaukonis, and L. Svilainis, "Air-coupled ultrasound spectroscopy air parameters compensation technique," *IEEE Sensors J.*, vol. 24, no. 8, pp. 12667–12675, Apr. 2024, doi: 10.1109/JSEN.2024.3369508.

[49] Y. Wang, K. Metzger, D. N. Stephens, G. Williams, S. Brownlie, and M. O'Donnell, "Coded excitation with spectrum inversion (CEXSI) for ultrasound array imaging," *IEEE Trans. Ultrason., Ferroelectr., Freq. Control*, vol. 50, no. 7, pp. 805–823, Jul. 2003, doi: 10.1109/TUFFC.2003.1214501.

[50] M. Oelze, "Bandwidth and resolution enhancement through pulse compression," *IEEE Trans. Ultrason., Ferroelectr., Freq. Control*, vol. 54, no. 4, pp. 768–781, Apr. 2007, doi: 10.1109/TUFFC.2007.310.

[51] G. S. Jeng, S. Huang, P. C. Li, and J. Tsao, "A novel pulse compression technique using inverse filtering in frequency domain," in *Proc. IEEE IUS*, Atlanta, GA, USA, Oct. 2001, pp. 1535–1538.

[52] J. Ruprecht and M. Rupf, "On the search for good aperiodic binary invertible sequences," *IEEE Trans. Inf. Theory*, vol. 42, no. 5, pp. 1604–1612, Sep. 1996, doi: 10.1109/18.532908.

[53] L. Svilainis, K. Lukoseviciute, and D. Liaukonis, "Reiterative deconvolution: New technique for time of flight estimation errors reduction in case of close proximity of two reflections," *Ultrasonics*, vol. 76, pp. 154–165, Apr. 2017, doi: 10.1016/j.ultras.2017.01.003.

[54] M. Sanchez, D. Gallego, A. A. Oraevsky, and H. Lamela, "A laser ultrasound emitter based on high-power diode laser in overdrive operation mode for biomedical imaging applications," *Ultrasonics*, vol. 148, Apr. 2025, Art. no. 107548, doi: 10.1016/j.ultras.2024.107548.

[55] D. Vangi, A. Virga, and M. S. Gulino, "Random sequence for optimal low-power laser generated ultrasound," *J. Phys., Conf. Ser.*, vol. 882, Jun. 2017, Art. no. 012013, doi: 10.1088/1742-6596/882/1/012013.

[56] L. Svilainis, A. Chaziachmetovas, V. Eidukynas, A. Aleksandrovas, and M. Varatinskas, "Compact laser driver for ultrasonic arbitrary position and width pulse sequences generation," *IEEE Trans. Instrum. Meas.*, vol. 70, pp. 1–15, 2021, doi: 10.1109/TIM.2021.3120144.